Journal of Physics A:
Mathematical and Theoretical

**PAPER**

# The flexibility in choosing distinct Green's functions for the boundary wall method: waveguides and billiards

To cite this article: F Teston *et al* 2022 *J. Phys. A: Math. Theor.* **55** 175201

View the article online for updates and enhancements.

You may also like

- Implementation of an Efficient Bayesian Search for Gravitational-wave Bursts with Memory in Pulsar Timing Array Data
Jerry Sun, Paul T. Baker, Aaron D. Johnson et al.
- The Mass Relations between Supermassive Black Holes and Their Host Galaxies at 1 < *z* < 2 with *HST*-WFC3
Xuheng Ding, John Silverman, Tommaso Treu et al.
- Fundamental Plane of Black Hole Activity in the Quiescent Regime
Fu-Guo Xie and Feng Yuan

This content was downloaded from IP address 186.217.191.178 on 29/02/2024 at 17:20

**IOP** Publishing Journal of Physics A: Mathematical and Theoretical

J. Phys. A: Math. Theor. **55** (2022) 175201 (23pp) https://doi.org/10.1088/1751-8121/ac5b90

# The flexibility in choosing distinct Green's functions for the boundary wall method: waveguides and billiards

**F Teston[1,3], A L Azevedo[1,3], M R Sales[1,2], F M Zanetti[1] and M G E da Luz[1,*]**

[1] Departamento de Física, Universidade Federal do Paraná, Curitiba-PR, 81531-980, Brazil

[2] Departamento de Física, Universidade Estadual de Ponta Grossa, Ponta Grossa-PR, 84030-900, Brazil

E-mail: luz@fisica.ufpr.br

Received 2 August 2021, revised 24 February 2022
Accepted for publication 8 March 2022
Published 4 April 2022

CrossMark

**Abstract**

The boundary wall method (BWM) is a general purpose protocol to treat boundary value problems for wave equations, specially Helmholtz's (the case addressed here). Similarly to most approaches, the BWM may be computationally demanding for large borders $\mathcal{C}$, at which the wave function must satisfy specified boundary conditions. Also, despite the fact the BWM is an exact procedure, usually it is not amenable to closed form solutions. The BWM relies on the Green's function $G_0$ of the embedding domain $V$ of $\mathcal{C}$. However, in many instances—like for $\mathcal{C}$ modeling a billiard—the specific $V$ is not really fundamental and thus one has a certain freedom to choose distinct domains and so $G_0$'s. Here we consider this characteristic of the BWM and show how to obtain some analytical results and solve numerically semi-infinite waveguides by exploring proper Green's functions. As examples, we discuss rectangular, triangular and trapezoidal structures with both Dirichlet and leaking boundaries as well as scattering states within semi-infinite rectangular waveguides.

Keywords: boundary wall method, wave equation, Green's function, quantum billiards, leaking borders

*Author to whom any correspondence should be addressed.

[3]These authors contributed equally to this work.

 © 2022 IOP Publishing Ltd Printed in the UK 

## 1. Introduction

It is needless to emphasizes the relevance of boundary value problems in physics [1, 2]. In fact, more broadly in almost all basic and applied areas of science one can find important phenomena modeled by partial differential equations obeying specific boundary conditions (BCs). This has prompted a large literature on the topic (for a very short glimpse see, e.g., [3–7]), motivating the development of innumerous analytic [8] and numerical [9] procedures to treat such a huge class of systems.

Certainly, a fundamental family of boundary value problems is that associated to undulatory behavior [10]. Among the many existing exact approaches to solve wave equations [11] (and in this contribution we concentrate on the Helmholtz operator, namely, $\nabla^2 + k^2$), the boundary wall method (BWM), proposed more two decades ago [12], is particularly distinct in the way it handles the BCs, which can be Dirichlet, Neumann, mixed or Robin [1], as well as leaking borders [13]. In the BWM, the connected or disconnected, open or closed, spatial frontiers of the system are viewed as sharp-walled boundaries $\mathcal{C}$'s (e.g., $\mathcal{C}_1$, $\mathcal{C}_2$ and $\mathcal{C}_3$ depicted in figure 1) and described by $\delta$-wall potentials (details in section 2). Thus, by assuming $\mathcal{C}$ an effective potential, one can consider the Lippmann–Schwinger equation [10, 14] to solve the problem. The correct BCs are achieved by means of proper features assumed for the $\delta$-wall potentials. Despite its scattering-like character, for $\mathcal{C}$ a closed shape, say a billiard, the BWM properly leads to the correct eigenstates and eigenenergies of the $\mathcal{C}$ inner region. A pertinent technical advantage is that the resulting integral equation—running just on the contour $\mathcal{C}$, instead over the full spatial domain $V$, and involving the 'free' Green's function $G_0$ of $V$—yields, for each wavenumber $k$, the wave solution $\psi_k(\mathbf{r})$ everywhere in $V$. For instance, for billiards there is no need for an 'inside' and an 'outside' integral equation, like in the boundary integral method.

A very comprehensive mathematical and numerical (for this latter see also [12]) review of the BWM can be found in [15]. For instance, reference [15] discusses that formally the framework corresponds to a reformulation of standard single-layer boundary integral methods [4], leading to a first-kind Fredholm equation (a feature of the BWM recently used in concrete calculations [16, 17]). Further conceptual aspects of the BWM have been examined in [18]. Also, the BWM is valid in any spatial dimension (see, e.g., [12, 19]). The BWM has been employed in many distinct applications, as for the investigation of matter waves [20–22], analysis of diverse optical processes [23–26] and description of certain nanostructure properties [18, 27, 28].

The different usages mentioned above illustrates the versatility of the BWM. But similarly to many boundary value problem protocols [4, 5], some issue for the BWM may also arise. Here we mention the eventually two most important ones. First, the great majority of the studies employing the BWM are numerical. Indeed, one of the main advantages of the approach is its straightforward numerical implementation [12, 15, 21, 24]. Nevertheless, the necessary computational work may be demanding if the linear lengths associated to $\mathcal{C}$ are too long compared to the typical wavelengths $\lambda = 2\pi/k$ considered, e.g., if one shall simulate very long waveguides in the regime of high frequency modes—refer to [18]. Second, there are just few exact analytical results derived with the BWM. We can cite straight lines [12] and circles [12, 18], with this latter shape being recently revisited in terms of particular integral equation solution techniques applied to the BWM [16]. Moreover, a 2D elliptical billiard [17] (for numerics see [27]) and a 3D spheroidal barrier [19] have being analyzed through ingenious transformations and appropriate coordinate system choices for the BWM associated expressions. In all these cases, $V$ is taken as the whole 2D or 3D space, thus with the polar or spherical symmetries of $G_0$ greatly complying with those of the investigated $\mathcal{C}$'s. Unfortunately, such type of symmetry

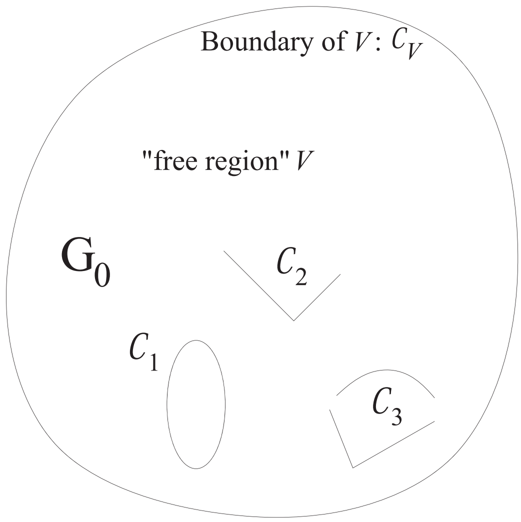


**Figure 1.** The BWM assumes that for the 'free region' $V \in \mathbb{R}^N$, the Green's function is given by $G_0$, where proper BCs are imposed on the borders $\mathcal{C}_V$ of $V$. If $\mathcal{C}_V$ goes to infinite, then $V = \mathbb{R}^N$ and $G_0$ is in fact the Green's function for the whole free space, the situation usually considered in the BWM. By describing arbitrary closed (e.g., $\mathcal{C}_1$), open connected (e.g., $\mathcal{C}_2$), and open disconnected (e.g., $\mathcal{C}_3$) sharp-walled structures—which can satisfy distinct BCs—as $\delta$-wall potentials, the BWM is able to obtain outside scattering and/or inside bound states in terms of a scattering approach based on a Lippmann–Schwinger-like equation.

matching, greatly mitigating the mentioned explicit computations, cannot be explored, e.g., for rectangular, cubic, etc, structures using these same $G_0$'s.

A totally unexplored ingredient of the BWM is that it does not demand the original domain $V$, in which $\mathcal{C}$ is embedded, to be the entire free $\mathbb{R}^N$. Actually, there is a great freedom (once some conditions are observed, section 2.1) to select $V$. Therefore, depending on the particular $\mathcal{C}$, one might try to choose $V$ such that (i) the corresponding $G_0$ is easy to obtain and (ii) the exact form of $G_0$ simplifies either analytically or numerically the calculations with the BWM. Given such perspective, our goal in the present contribution is to show how proper $V$'s—more concretely, the interior of semi-infinite waveguides—lead to Green's functions which considerably facilitates the analysis of distinct $\mathcal{C}$'s using the BWM. Our general considerations here are valid for arbitrary dimensions. But for the concrete examples we present along the work, we focus just on the 2D case.

The paper is organized as the following. In section 2 we present a short overview on the BWM, also explaining how it can be implemented supposing distinct $V$'s, thence $G_0$'s. In section 3 we discuss a general prescription to derive the exact Green's function for certain types of semi-infinite waveguides, useful for our purposes. As an illustration we consider the rectangular semi-infinite waveguide in 2D. In section 4 we assume the waveguide domain $V$ explicitly calculated in section 3 and examine different applications. We obtain analytical results for both a rectangular billiard and a waveguide with a permeable resonant structure in its extreme. Numerical eigenstates and eigenvalues are computed for right triangle and square trapezium billiards as well as for a waveguide with a permeable triangular billiard at its ending. The conclusion is drawn in section 5.

## 2. A brief summary of the BWM

The BWM construction has been fully developed in [12, 15]. So, here we just outline the main ideas and the most relevant results without going into much details. We assume the Helmholtz equation in $V \in \mathbb{R}^N$, with appropriate BCs at $\mathcal{C}_V$, see figure 1. In the case of $\mathcal{C}_V$ tending to infinity, we have the actual free whole space and the BCs would correspond either to the outgoing (+) or to the incoming (−) radiation condition. In the (empty) $V$ region, the incident (or initial or 'seed' [15]) wave function $\phi_k(\mathbf{r})$ satisfies $(\nabla^2 + k^2)\phi_k(\mathbf{r}) = 0$, whereas the 'free' (0) Green's function is given by $(\nabla^2 + k^2)G_0(\mathbf{r}, \mathbf{r}_0; k) = \delta(\mathbf{r} - \mathbf{r}_0)$. For relevant literature on general aspects of Green's functions we can cite, for example, references [29–32]. The desired BCs at $\mathcal{C}_V$ must be imposed to both $\phi_k(\mathbf{r})$ and $G_0(\mathbf{r}, \mathbf{r}_0; k)$. Here $k^2 = E$ (with $\hbar^2/(2\mu) = 1$).

Now, for $U$ a compact support potential within the region $V$, the scattering wave solution $\psi_k(\mathbf{r})$ for the problem is given by the Lippmann–Schwinger equation $\psi_k(\mathbf{r}) = \phi_k(\mathbf{r}) + \int_V \mathrm{d}\mathbf{r}_0 G_0(\mathbf{r}, \mathbf{r}_0; k) U(\mathbf{r}_0)\psi_k(\mathbf{r}_0)$. The BWM essential idea [12] is then to write $U(\mathbf{r})$ as the $\delta$-wall potential $U(\mathbf{r}) = \int_{\mathcal{C}} \mathrm{d}s\gamma(s)\delta(\mathbf{r} - \mathbf{r}(s))$, where $s$ parameterizes all the points along the sharp-walled curve $\mathcal{C}$, with $\mathbf{r}(s)$ being their vector positions. Here $\gamma(s)$ gives the permeability (or leakage) of $\mathcal{C}$ at each point $s$. Actually, if one assumes a plane wave of wavenumber $k$, incident perpendicular to the point $s$ on $\mathcal{C}$, then it has the probability $P_t = 4k^2/(4k^2 + \gamma(s)^2)$ to be transmitted through and $P_r = \gamma(s)^2/(4k^2 + \gamma(s)^2)$ to be reflected from $s$. In the limit $\gamma \to \infty$ (so that $P_t = 0$) one can show that $\psi_k$ does vanish on $\mathcal{C}$ [12], corresponding to the usual Dirichlet BC. Other BCs, like Neumann, mixing and Robin, are also possible by setting other $\delta$-like expressions [33] for $U$ (the reader is referred to [12], in particular its appendix B, for a throughout discussion). In this work we concentrate only in uniformly permeable, thus with $\gamma$ a constant along the whole $\mathcal{C}$, and Dirichlet BCs.

By inserting the above $U$ into the Lippmann–Schwinger equation one gets ($\mathbf{r} \in V$)

$$\psi_k(\mathbf{r}) = \phi_k(\mathbf{r}) + \gamma \int_{\mathcal{C}} \mathrm{d}s G_0(\mathbf{r}, \mathbf{r}(s); k)\psi_k(\mathbf{r}(s)). \tag{1}$$

In a close relation with the standard $T$-matrix in formal scattering theory [14], one can define $\psi_k(\mathbf{r}(s'')) = \int_{\mathcal{C}} \mathrm{d}s' T_\gamma(s'', s'; k)\phi_k(\mathbf{r}(s'))$, such that

$$\psi_k(\mathbf{r}) = \phi_k(\mathbf{r}) + \gamma \int_{\mathcal{C}}\int_{\mathcal{C}} \mathrm{d}s''\, \mathrm{d}s' G_0(\mathbf{r}, \mathbf{r}(s''); k) T_\gamma(s'', s'; k)\phi_k(\mathbf{r}(s')). \tag{2}$$

A series representation for $T_\gamma$ yields [15]

$$T_\gamma(s'', s'; k) = \delta(s'' - s') + \sum_{j=1}^{\infty} T_\gamma^{(j)}(s'', s'; k), \tag{3}$$

where

$$\begin{aligned} T_\gamma^{(j)}(s'', s'; k) = \gamma^j \int \mathrm{d}s_1\, \mathrm{d}s_2 \ldots \mathrm{d}s_{j-1} G_0(\mathbf{r}(s''), \mathbf{r}(s_{j-1}); k) \\ \times G_0(\mathbf{r}(s_{j-1}), \mathbf{r}(s_{j-2}); k) \ldots G_0(\mathbf{r}(s_1), \mathbf{r}(s'); k). \end{aligned} \tag{4}$$

For the particular case of $\gamma \to \infty$ we can proceed as the following. By defining $T(s'', s'; k) = -\lim_{\gamma\to\infty} \gamma\, T_\gamma(s'', s'; k)$, it reads [18]

$$\delta(s'' - s') = \int_{\mathcal{C}} \mathrm{d}s T(s'', s; k) G_0(\mathbf{r}(s), \mathbf{r}(s'); k)$$
$$= \int_{\mathcal{C}} \mathrm{d}s G_0(\mathbf{r}(s''), \mathbf{r}(s); k) T(s, s'; k), \tag{5}$$

and for any $\mathbf{r} \in V$

$$\psi_k(\mathbf{r}) = \phi_k(\mathbf{r}) - \int_{\mathcal{C}} \int_{\mathcal{C}} \mathrm{d}s'' \, \mathrm{d}s' G_0(\mathbf{r}, \mathbf{r}(s''); k) T(s'', s'; k) \phi_k(\mathbf{r}(s')). \tag{6}$$

For $\mathbf{r}$ in $\psi_k(\mathbf{r})$ taken as a vector position $\mathbf{r}(s)$ of an arbitrary $s$ on $\mathcal{C}$, from equation (5) into equation (6) we find that $\psi_k(\mathbf{r}(s))$ identically vanishes, thus satisfying the Dirichlet BC as previously anticipated.

A first remarkable property of the BWM for a closed $\mathcal{C}$, a billiard, is the so called filter mechanism [15]. Assume $\{k_n, \Psi_n\}$ the set of eigensolutions of the interior of $\mathcal{C}$. Such mechanism guarantees that for any $\mathbf{r}$ in the inner region: (i) if $k \neq k_n$, then the method naturally gives $\psi_k(\mathbf{r}) = 0$ (although in the outside region $\psi_k$ is the correct scattering solution, with $\phi_k$ corresponding to the incident wave); (ii) if $k = k_n$ for some $n$ and for $\phi_k$ displaying proper symmetry conditions (see [15]), we have $\psi_k(\mathbf{r}) = \Psi_n(\mathbf{r})$.

A second, very handy, feature of the BWM is that to find the set of $k_n$'s of a billiard one does not need to calculate the $\psi_k$'s. As described in [12, 18], for $k$ approaching a $k_n$, $T(k)$ starts to present very special characteristics, easily identifying a resonant $k$, i.e., an eigenwavenumber. Thus, varying $k$ in $T(k)$ is the common procedure to determine the spectrum of a billiard through the BWM.

As already pointed out in the introduction, the BWM numerical formulation is relatively simple and well discussed in the literature (for instance, a step by step recipe with the necessary explicit formulas are given in [15]). In a nutshell, one discretizes $\mathcal{C}$ so the function $T$ becomes a square matrix, computed from a matrix version of equation (5) (or from its finite $\gamma$ version, cf, equation (9) in [12]). Then, equation (2) or equation (6) can be solved by means of direct quadratures. Fundamental for our purposes is that such scheme is independent on the actual functional form of $G_0$, unless of course for the particularities of its numerical calculation. Therefore, for distinct $G_0$'s the same existing numerical algorithms for the BWM can be used without appreciable modifications.

### 2.1. The choice of the spatial domain $V$

It may be the case one shall address specific undulatory behavior associated uniquely to the shape $\mathcal{C}$ and for which the embedding $V$ in principle should not be relevant. For example, the inside eigenstates for $\mathcal{C}$ a billiard or the outside scattering features in the close proximity of an arbitrary $\mathcal{C}$ [34–36]. Hence, provided $V$ is consistent with the investigated phenomenon, there is great flexibility in its choice for the BWM.

This motivates to look for domain geometries facilitating the analysis. Just as an illustration, suppose one wishes to discuss a process like the scattering resonances of two impenetrable disks in the plane [37, 38] (modeled as circles with Dirichlet BCs). Using the BWM, one possible strategy could be to consider the Green's function for the 2D free space—$G_0^{(+)}(\mathbf{r}, \mathbf{r}_0; k) = -\frac{\mathrm{i}}{4} H_0^{(+)}(k|\mathbf{r} - \mathbf{r}_0|)$—and then take $\mathcal{C}$ as the two circles. Nonetheless, apart from the numerical handling of $G_0$, the necessary numerical work (to obtain $T$ and to perform the integrals for $\psi_k$)

in this first approach would be reduced if instead, we assume as $G_0$ the Green's function for the exterior region of a circle in 2D[4] and thus $\mathcal{C}$ only as the second circle.

A key point mentioned above regards the compatibility between the sought solutions $\psi_k$ with the domain $V$. Such aspect of the BWM is easy to comprehend supposing $\mathcal{C}$ a closed curve, like $\mathcal{C}_1$ in figure 1. Consider we are trying to determine the eigenstates and eigenvalues of $\mathcal{C}$. If $V$ is also limited (e.g., figure 1), the possible $k$'s from the 'seed' states $\phi_k$ (see the method description) are those belonging to the spectrum of the Helmholtz equation on $V$, $\{k_n\}_V$. Therefore, using the BWM we cannot obtain the solutions for a billiard $\mathcal{C}$ within an also closed $V$ if $\{k_n\}_{\mathcal{C}}$ and $\{k_n\}_V$ are distinct. To avoid the problem, one should set $V$ as an open region, moreover displaying symmetries conforming with those of $\mathcal{C}$.

However, bearing the above in mind, proper selections of $V$'s could broaden the applicability of the BWM. For instance, allowing to treat much longer $\mathcal{C}$'s, reducing the necessary computational efforts to solve closed shapes, and even to open the possibility of analytical results—presently limited to very few cases once the practice in the literature is to set $V = \mathbb{R}^N$. So, among potential candidates for $V$'s we mention semi-infinite or infinite waveguide-like geometries. Generally speaking, they are finite in all directions but one, along which extending over $\mathbb{R}_+$ or $\mathbb{R}$.

In the next section we describe a general method to obtain the exact Green's function for a certain class of semi-infinite waveguides, which are very suitable for the BWM. We further solve a particular example, a rectangular shape. Section 4 is then dedicated to explore such particular domain.

## 3. The Green's function for semi-infinite waveguides

Next we address the outgoing $(+)$ and incoming $(-)$ Green's function $G^{(\pm)}$ for the Helmholtz operator $\hat{\mathcal{L}}_k^V \equiv \nabla_{\mathbf{r}}^2 + k^2$ defined on $V \in \mathbb{R}^N$ [31]. We concentrate only on Dirichlet BCs at the frontiers $\mathcal{C}_V$ of $V$. The procedure next is aimed to a particular type of semi-infinite waveguide structure, for which $V = (0, \infty) \times \Omega$, with $\Omega$ a limited (finite) region of $\mathbb{R}^{N-1}$. Owed to the specific geometry of $V$, we can assume there exists a coordinate system allowing to write $(0 < \xi < \infty, \boldsymbol{\eta} = (\eta_1, \eta_2, \ldots, \eta_{N-1}), a_n < \eta_n < b_n$ for $a_n < b_n$ finites $\forall n$, and $\mathbf{r} = (\xi, \boldsymbol{\eta}))$

$$\begin{aligned}\hat{\mathcal{L}}_k^V G(\xi, \boldsymbol{\eta}; \xi_0, \boldsymbol{\eta}_0; k) &= \left(\hat{\mathcal{O}}_\xi + f(\xi)\nabla_{\boldsymbol{\eta}}^2 + k^2\right) G(\xi, \boldsymbol{\eta}; \xi_0, \boldsymbol{\eta}_0; k) = \delta(\mathbf{r} - \mathbf{r}_0) \\ &= s(\xi)\delta(\xi - \xi_0)\delta(\boldsymbol{\eta} - \boldsymbol{\eta}_0),\end{aligned} \tag{7}$$

where $\hat{\mathcal{O}}_\xi = f_2(\xi)\partial^2/\partial\xi^2 + f_1(\xi)\partial/\partial\xi + f_0(\xi)$ [29, 30]. Note that $\hat{\mathcal{O}}_\xi$ should be related to wave-like solutions since it is somehow the component of the Helmholtz equation along the semi-infinite direction $\xi$.

We have $G(\xi, \boldsymbol{\eta} \in \mathcal{C}_\Omega; \xi_0, \boldsymbol{\eta}_0; k) = 0$ and depending on each particular $\mathcal{C}_V$, a specific condition for $G(0, \boldsymbol{\eta}; \xi_0, \boldsymbol{\eta}_0; k)$ must also be observed (see the explicit example in the following). Moreover, given that $\hat{\mathcal{L}}_k$ is a second order differential operator, $G$ is continuous at $\mathbf{r} = \mathbf{r}_0$, but across $\mathbf{r}_0$ displaying finite jumps in its first derivatives which yield a delta function-like divergence for the second derivatives (see, e.g., [39]). We seek $\pm$ solutions (with $+$ corresponding to

[4] The exact outgoing Green's function for the exterior of a circle of radius $R$ centered at the origin and satisfying Dirichlet BCs reads $G_0^{(+)}(\mathbf{r}, \mathbf{r}_0; k) = -\frac{\mathrm{i}}{4}H_0^{(+)}(k|\mathbf{r} - \mathbf{r}_0|) + \frac{\mathrm{i}}{4}\frac{J_0(kR)}{H_0^{(+)}(kR)}H_0^{(+)}(kr)H_0^{(+)}(kr_0) + \frac{\mathrm{i}}{2}\sum_{n=1}^{\infty}\frac{J_n(kR)}{H_n^{(+)}(kR)}H_n^{(+)}(kr)H_n^{(+)}(kr_0)\cos[n(\theta - \theta_0)]$, where $J_n$ and $H_n^{(+)}$ are the Bessel and first kind Hankel functions of order $n$. Maybe surprisingly, the infinite series can be numerically computed with the help of asymptotic expansions in the order parameter $n$ (see, e.g., reference [15]).

the Sommerfeld radiation condition), so $G^{(\pm)}(\xi \to \infty) \sim (1/\sqrt{\xi^{(N-1)d}}) \exp[\pm \mathrm{i}k\xi]$ for $d$ related to the degree of separability of $\xi$ and $\boldsymbol{\eta}$ (e.g., if $f(\xi) = 1$ then $d = 0$) [30].

For the limited region $\Omega$, the Helmholtz operator $\hat{\mathcal{L}}_{\tilde{k}}^{\Omega} = \nabla_{\boldsymbol{\eta}}^2 + \tilde{k}^2$ represents an eigenvalue problem, such that [40] (with $n = 1, 2, \ldots,$ labeling the distinct eigenmodes)

$$\begin{aligned} \left(\nabla_{\boldsymbol{\eta}}^2 + k_n^2\right) w_n(\boldsymbol{\eta}) &= 0, \\ w_n(\boldsymbol{\eta} \in \mathcal{C}_\Omega) &= 0, \\ \int_\Omega \mathrm{d}\boldsymbol{\eta} w_{n_2}(\boldsymbol{\eta}) w_{n_1}^*(\boldsymbol{\eta}) &= \delta_{n_2 n_1}, \\ \sum_n w_n(\boldsymbol{\eta}_2) w_n^*(\boldsymbol{\eta}_1) &= \delta(\boldsymbol{\eta}_2 - \boldsymbol{\eta}_1), \end{aligned} \tag{8}$$

with the last identity above representing the completeness relation of the $w_n$'s in $\Omega$ [40].

Due to the form of $\hat{\mathcal{L}}_k^V$ in equations (7) and (8), it is natural to write

$$G(\xi, \boldsymbol{\eta}; \xi_0, \boldsymbol{\eta}_0; k) = \sum_n w_n(\boldsymbol{\eta}) w_n^*(\boldsymbol{\eta}_0) F_n(\xi; \xi_0; k), \tag{9}$$

demanding that for any $n$

$$\left(\hat{\mathcal{O}}_\xi - f(\xi)k_n^2 + k^2\right) F_n(\xi; \xi_0; k) = s(\xi)\delta(\xi - \xi_0). \tag{10}$$

When $\xi \neq \xi_0$ (so $\delta(\xi - \xi_0) = 0$), the resulting homogeneous second order differential equation—$\left(\hat{\mathcal{O}}_\xi - f(\xi)k_n^2 + k^2\right) \mathcal{F}_n(\xi; k) = 0$—does admit two fundamental (stationary wave) solutions [29, 40], $\mathcal{F}_n = u_n(\xi; k)$ and $\mathcal{F}_n = v_n(\xi; k)$. In principle, correct linear combinations of these functions—say, $h_n^{(\pm)}(\xi; k) = \alpha_n u_n(\xi; k) \pm \mathrm{i}\beta_n v_n(\xi; k)$—should asymptotically represent proper outgoing and incoming waves.

In this way, assuming that $u_n(\xi; k)$ leads to the desired condition for $G^{(\pm)}$ at $\xi = 0$, we can take $F_n^{(\pm)} \propto u_n(\xi; k)$ for $\xi < \xi_0$ and $F_n^{(\pm)} \propto h_n^{(\pm)}(\xi; k)$ for $\xi > \xi_0$. Then, it is straightforward to realize that a continuous $F$ at $\xi = \xi_0$, but presenting a 'leap' in its first derivative, reads (for $C_n^{(\pm)}$ a constant and $\xi_>$ ($\xi_<$) the larger (smaller) between $\xi$ and $\xi_0$)

$$F_n^{(\pm)}(\xi; \xi_0; k) = C_n^{(\pm)} u_n(\xi_<; k) h_n^{(\pm)}(\xi_>; k). \tag{11}$$

The last step is to determine $C_n^{(\pm)}$ in order to comply with equation (10). With this aim, we divide equation (10) by $f_2(\xi)$, integrate the resulting expression in $\xi$ from $\xi_0 - \epsilon$ to $\xi_0 + \epsilon$ and take the limit $\epsilon \to 0$. By using the fact that $F$ is continuous and employing integration by parts for the term of $\hat{\mathcal{O}}_\xi$ involving $\partial/\partial\xi$, we get (with $z'(\xi) \equiv \mathrm{d}z(\xi)/\mathrm{d}\xi$ and $W[z_2(\xi), z_1(\xi)] \equiv z_2'(\xi) z_1(\xi) - z_2(\xi) z_1'(\xi)$ the Wronskian of $z_2(\xi)$ and $z_1(\xi)$)

$$C_n^{(\pm)} = \frac{s(\xi_0)}{f_2(\xi_0)} \frac{1}{W[h_n^{(\pm)}(\xi_0; \xi_0; k), u_n(\xi_0; \xi_0; k)]}. \tag{12}$$

Finally, we observe that from the above the BCs for $G$ are also observed in the variables $\mathbf{r}_0$, as it should be because the symmetry $\mathbf{r} \leftrightarrow \mathbf{r}_0$ in the Green's function equation [31, 39].

### 3.1. The rectangular semi-infinite waveguide

To illustrate the previous prescription, we consider the geometry depicted in figure 2(a). It corresponds to a rectangular semi-infinite waveguide region $0 < y < L_y$, $x > 0$, for which

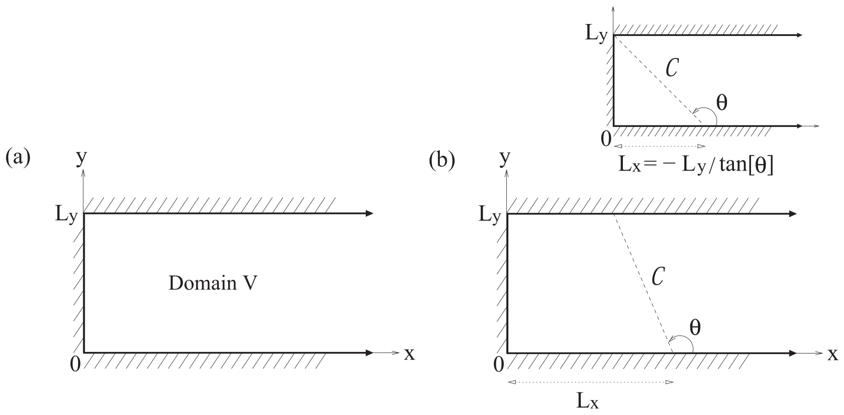


**Figure 2.** (a) The domain $V$ of a rectangular semi-infinite waveguide in 2D. (b) The straight line $\mathcal{C}$ together with parts of the walls of $V$ can form distinct billiard shapes, like a rectangular trapezium, a rectangle (if $\theta = \pi/2$), and a right triangle if $L_x$ is properly set (top right corner detail).

we impose Dirichlet BCs at $y = 0$, $y = L_y$ and $x = 0$. So we can use Cartesian coordinates, with $\nabla^2_{\mathbf{r}} = \partial^2/\partial x^2 + \partial^2/\partial y^2$ and $\delta(\mathbf{r} - \mathbf{r}_0) = \delta(x - x_0)\delta(y - y_0)$. Also, $G(0, y; x_0; y_0; k) = G(x, 0; x_0; y_0; k) = G(x, L_y; x_0; y_0; k) = 0$. For the limited direction $y$ ($n = 1, 2, \ldots$)

$$\varphi_n^{(L_y)}(y) = \sqrt{\frac{2}{L_y}}\,\sin\left[\frac{n\pi y}{L_y}\right], \quad \frac{\mathrm{d}^2}{\mathrm{d}y^2}\varphi_n^{(L_y)}(y) + \frac{n^2\pi^2}{L_y^2}\varphi_n^{(L_y)}(y) = 0, \tag{13}$$

where $\varphi_n^{(L_y)}(0) = \varphi_n^{(L_y)}(L_y) = 0$. In this case the solutions for the homogeneous version of equation (10) are $\sin[k_n x]$, $\cos[k_n x]$, and $\exp[\pm \mathrm{i} k_n x]$, with $k_n^2 = k^2 - n^2\pi^2/L_y^2$. Hence, to observe the boundary condition at $x = 0$ we set $u_n(x) = \sin[k_n x]$ (obviously $h_n^{(\pm)}(x) = \exp[\pm \mathrm{i} k_n x]$). Lastly, $W[\exp[\pm \mathrm{i} k_n x_0],\ \sin[k_n x_0]] = -k_n$ and therefore the exact Green function for the rectangular semi-infinite waveguide reads

$$G^{(\pm)}_{\mathrm{rwg}}(x, y; x_0, y_0; k) = \sum_{n=1}^{\infty} \varphi_n^{(L_y)}(y)\varphi_n^{(L_y)}(y_0)\frac{(-1)}{k_n}\sin[k_n x_<]\exp[\pm \mathrm{i} k_n x_>], \tag{14}$$

where $k_n = \sqrt{k^2 - n^2\pi^2/L_y^2}$, $\varphi_n^{(L_y)}(z) = \sqrt{2/L_y}\,\sin[n\pi z/L_y]$ and $x_>$ ($x_<$) is the greater (smaller) between $x$ and $x_0$. The superscript $+(-)$ means the outgoing (incoming) case.

As a very instructive exercise, in the appendix A we show how to obtain the usual Green's function for a 2D box from the present $G^{(\pm)}_{\mathrm{rwg}}$ solutions.

## 4. Applications for the domain $V$ as the rectangular semi-infinite waveguide

Let us suppose a segment of line $\mathcal{C}$ within the region $V$, figure 2(b), whose parametric equation is (for $0 \leqslant t \leqslant 1$)

$$x(t) = L_x + \frac{L_y}{\tan[\theta]}t, \quad y(t) = L_y t. \tag{15}$$

Note that here $t$ plays the same role than $s$ in section 2.

Such single $\mathcal{C}$, when considered together with parts of the $V$ border, form some simple polygonal billiards. Indeed, for an arbitrary $L_x$, $\mathcal{C}$ leads—with the waveguide walls—to a rectangular trapezoidal shape, whereas by setting $L_x = -L_y/\tan[\theta]$, we have a right triangle (as illustrated in the inset of figure 2(b)). Finally, a rectangular structure emerges when $\theta = \pi/2$, so that $\tan[\theta] \to \infty$ and then $x(t) = L_x$ and $y(t) = L_y t$.

In section 4.2 we numerically calculate $\psi_k(\mathbf{r})$ for the systems of figure 2(b), assuming distinct permeabilities $\gamma$ and geometric parameters $L_x$ and $\theta$ for $\mathcal{C}$. But prior to that, we present next some analytically solvable examples.

### 4.1. Analytical results for $\mathcal{C}$ with $\theta = \pi/2$

*4.1.1. The T and $T_\gamma$ matrices.* We set $\theta = \pi/2$ and assume Dirichlet BCs on $\mathcal{C}$. The expression for the $T$ matrix, second relation in equation (5), with $G_0$ given by $G^{(\pm)}_{\mathrm{rwg}}$ in equation (14), yields (for $0 \leqslant t_b, t_a \leqslant 1$)

$$\delta(t_b - t_a) = \int_0^1 \mathrm{d}t \sum_{n=1}^{\infty} \varphi_n(L_y t_b)\varphi_n(L_y t) \frac{(-1)}{k_n} \sin[k_n L_x] \exp[\pm \mathrm{i} k_n L_x]\, T^{(\pm)}(t, t_a; k). \tag{16}$$

Above we have dropped the superscript $(L_y)$ in $\varphi$ for notation simplicity. Recalling that

$$\int_0^1 \mathrm{d}t \varphi_n(L_y t)\varphi_m(L_y t) = \frac{1}{L_y}\delta_{nm},$$
$$\sum_{n=1}^{\infty} \varphi_n(L_y t_b)\varphi_n(L_y t_a) = \frac{1}{L_y}\delta(t_b - t_a), \tag{17}$$

then by a direct inspection of equation (16) we find

$$T^{(\pm)}(t_b, t_a; k) = -L_y^2 \sum_{n=1}^{\infty} \varphi_n(L_y t_b)\varphi_n(L_y t_a) \frac{k_n \exp[\mp \mathrm{i} k_n L_x]}{\sin[k_n L_x]}. \tag{18}$$

For the more general case of a permeable $\mathcal{C}$, of permeability constant $\gamma$, we also can obtain $T_\gamma^{(\pm)}$ in an exact closed form. Indeed, in the present case of $\theta = \pi/2$ we have for the Equation (4)

$$\begin{aligned} T_\gamma^{(\pm, j)}(t_b, t_a; k) = \gamma^j \int \mathrm{d}t_1\, \mathrm{d}t_2 \ldots \mathrm{d}t_{j-1} &\sum_{n_j n_{j-1} \ldots n_2 n_1} \frac{(-1)^j}{k_{n_j} k_{n_{j-1}} \ldots k_1} \\ &\times \varphi_{n_j}(L_y t_b)\varphi_{n_j}(L_y t_{j-1})\varphi_{n_{j-1}}(L_y t_{j-1})\varphi_{n_{j-1}}(L_y t_{j-2}) \\ &\times \varphi_{n_{j-2}}(L_y t_{j-2})\varphi_{n_{j-2}}(L_y t_{j-3}) \ldots \varphi_{n_3}(L_y t_3)\varphi_{n_3}(L_y t_2) \\ &\times \varphi_{n_2}(L_y t_2)\varphi_{n_2}(L_y t_1)\varphi_{n_1}(L_y t_1)\varphi_{n_1}(L_y t_a) \\ &\times \prod_{l=1}^{l=j} \sin[k_{n_l} L_x] \exp[\pm \mathrm{i} k_{n_l} L_x]. \end{aligned} \tag{19}$$

Taking into account the first relation in equation (17) for the successive integrals in equation (19), we get

$$T_\gamma^{(\pm, j)}(t_b, t_a; k) = \sum_{n=1}^{\infty} L_y \left( -\gamma \, \frac{\sin[k_n L_x] \exp[\pm \mathrm{i} k_n L_x]}{L_y k_n} \right)^j \times \varphi_n(L_y t_b)\varphi_n(L_y t_a). \tag{20}$$

Lastly, rewritten the $\delta$ function in equation (3) in terms of the second relation in equation (17), we find for $T_{\gamma}^{(\pm)}$

$$T_{\gamma}^{(\pm)}(t_b, t_a; k) = L_y \sum_{n=1}^{\infty} \sum_{j=0}^{\infty} \left( -\gamma \frac{\sin[k_n L_x] \exp[\pm \mathrm{i} k_n L_x]}{L_y k_n} \right)^j \varphi_n(L_y t_b) \varphi_n(L_y t_a)$$

$$= \sum_{n=1}^{\infty} \frac{L_y^2 k_n \varphi_n(L_y t_b) \varphi_n(L_y t_a)}{L_y k_n + \gamma \, \sin[k_n L_x] \exp[\pm \mathrm{i} k_n L_x]}. \tag{21}$$

Observe that as discussed in section 2, we readily obtain $T$ in equation (18) from $T_\gamma$ in equation (21) as $T = -\lim_{\gamma \to \infty} \gamma \times T_\gamma$.

*4.1.2. The solution $\psi_k$ for the Dirichlet BC.* A function $\phi_k(\mathbf{r})$ which solves the free semi-infinite waveguide (i.e., in the absence of $\mathcal{C}$) is given by

$$\phi_k(\mathbf{r}) = C_l \, \sin[l\pi y/L_y] \sin[k_l x], \tag{22}$$

where $l$ is a positive integer, $k^2 = k_l^2 + l^2\pi^2/L_y^2$ and $C_l$ is a proper normalization constant.

To calculate $\psi_k$ satisfying Dirichlet BCs on $\mathcal{C}$ we consider equation (6) with $T$ from equation (18). We have two cases, the internal ($x < L_x$) and external ($x > L_x$) regions. For the first ($\mathbf{r} = (x < L_x, y)$)

$$\psi_k(\mathbf{r}) = C_l \, \sin\left[\frac{l\pi y}{L_y}\right] \sin[k_l x] - \left\{ C_l \sum_{n,m=1}^{\infty} \sin\left[\frac{n\pi y}{L_y}\right] \sin[k_n x] \frac{k_m \, \exp[\pm \mathrm{i}(k_n - k_m)L_x]}{k_n \, \sin[k_m L_x]} L_y^2 \right.$$

$$\left. \times \int_0^1 \int_0^1 \mathrm{d}t_b \, \mathrm{d}t_a \varphi_n(L_y t_b) \varphi_m(L_y t_b) \varphi_m(L_y t_a) \varphi_l(L_y t_a) \right\} \sin[k_l L_x]$$

$$= C_l \, \sin\left[\frac{l\pi y}{L_y}\right] \sin[k_l x] - \left\{ C_l \sum_{n,m=1}^{\infty} \sin\left[\frac{n\pi y}{L_y}\right] \sin[k_n x] \right.$$

$$\left. \times \frac{k_m \, \exp[\pm \mathrm{i}(k_n - k_m)L_x]}{k_n \, \sin[k_m L_x]} \delta_{nm} \delta_{ml} \right\} \sin[k_l L_x]. \tag{23}$$

Here the filter mechanism mentioned in the section 2 becomes manifest. Suppose a wavenumber $k$ such that $k_l L_x = j\pi$ for some $j = 1, 2, \ldots$ (therefore $k^2 = \pi^2 \, (l^2/L_y^2 + j,^2/L_x^2)$). Thus $\sin[k_l L_x] = 0$, the second term in the rhs of the last relation in equation (23) vanishes and

$$\psi_k(\mathbf{r}) = C_l \, \sin[l\pi y/L_y] \sin[j\pi x/L_x] = \phi_k(\mathbf{r}), \tag{24}$$

which is the exact eigenstate for a 2D rectangular box. On the other hand, if $k_l \neq j\pi/L_x$ ($j$ integer) equation (23) yields

$$\psi_k(\mathbf{r}) = C_l \, \sin\left[\frac{l\pi y}{L_y}\right] \sin[k_l x] - C_l \, \sin\left[\frac{l\pi y}{L_y}\right] \sin[k_l x] = 0, \tag{25}$$

the correct trivial null solution since $k$ does not correspond to an eigenwavenumber for the inside problem.

For the outside region

$$\psi_k(\mathbf{r}) = C_l \sin\left[\frac{l\pi y}{L_y}\right]\sin[k_l x] - \left\{C_l \sum_{n,m=1}^{\infty} \sin\left[\frac{n\pi y}{L_y}\right]\exp[\pm \mathrm{i}k_n x]\frac{k_m \sin[k_n L_x]}{k_n \sin[k_m L_x]}\exp[\mp \mathrm{i}k_m L_x]L_y^2\right.$$
$$\left.\times\int_0^1\int_0^1 \mathrm{d}t_b\,\mathrm{d}t_a\varphi_n(L_y t_b)\varphi_m(L_y t_b)\varphi_m(L_y t_a)\varphi_l(L_y t_a)\right\}\sin[k_l L_x]$$
$$= C_l \sin\left[\frac{l\pi y}{L_y}\right]\sin[k_l x] - \left\{C_l \sum_{n,m=1}^{\infty} \sin\left[\frac{n\pi y}{L_y}\right]\exp[\pm \mathrm{i}k_n x]\right.$$
$$\left.\times\frac{k_m \sin[k_n L_x]}{k_n \sin[k_m L_x]}\exp[\mp \mathrm{i}k_m L_x]\delta_{nm}\delta_{ml}\right\}\sin[k_l L_x]. \tag{26}$$

Notice that if again we choose $k_l$ such that $\sin[k_l L_x] = 0$, the above outside $\psi_k(\mathbf{r})$ displays the same exact functional form of the inside $\psi_k(\mathbf{r})$, equation (24). This is a nice example of the transparency principle (TP) for billiards [41, 42, 43], taking place whenever there is a perfect symmetry matching of the inner eigenstates with the exterior scattering solutions. In the present example the TP is heuristically easy to understand. The vertical $\mathcal{C}$ is an infinitely repulsive $\delta$-wall barrier within the waveguide (located at $x = L_x$). However, it has zero width and since the incident wave vanishes exactly at $x = L_x$, then $\phi_k$ does not 'feel' such barrier potential. Hence, it is like the solution in equation (24) would extend everywhere in the semi-infinite rectangular waveguide, in agreement with equation (26).

Finally, when $\sin[k_l L_x] \neq 0$ we have from equation (26)

$$\psi_k(\mathbf{r}) = C_l \sin\left[\frac{l\pi y}{L_y}\right](\sin[k_l x] - \exp[\pm \mathrm{i}k_l(x - L_x)]\sin[k_l L_x])$$
$$= D_l^{(\pm)} \sin\left[\frac{l\pi y}{L_y}\right]\sin[k_l(x - L_x)], \tag{27}$$

which is the expected steady solution for the semi-infinite waveguide, just with the closed end moved from $x = 0$ to $x = L_x$ ($D_l^{(\pm)}$ is simply a redefined normalization constant).

*4.1.3. The solution $\psi_k$ for a permeable $\mathcal{C}$.* Now, for $\psi_k$ we consider equation (2) with $T_\gamma$ from equation (21). For $\phi_k$ we assume equation (22). For the internal ($x < L_x$) region

$$\psi_k(\mathbf{r}) = C_l \sin\left[\frac{l\pi y}{L_y}\right]\sin[k_l x] - \gamma C_l$$
$$\times\left\{\sum_{n,m=1}^{\infty} \sin\left[\frac{n\pi y}{L_y}\right]\sin[k_n x]\frac{(k_m/k_n)\exp[\pm \mathrm{i}k_n L_x]L_y^2}{k_m L_y + \gamma \sin[k_m L_x]\exp[\pm \mathrm{i}k_m L_x]}\right.$$
$$\left.\times\int_0^1\int_0^1 \mathrm{d}t_b\,\mathrm{d}t_a\varphi_n(L_y t_b)\varphi_m(L_y t_b)\varphi_m(L_y t_a)\varphi_l(L_y t_a)\right\}\sin[k_l L_x]$$
$$= C_l \sin\left[\frac{l\pi y}{L_y}\right]\sin[k_l x] - \left\{\gamma C_l \sum_{n,m=1}^{\infty} \sin\left[\frac{n\pi y}{L_y}\right]\sin[k_n x]\right.$$
$$\left.\times\frac{(k_m/k_n)\exp[\pm \mathrm{i}k_n L_x]}{k_m L_y + \gamma \sin[k_m L_x]\exp[\pm \mathrm{i}k_m L_x]}\delta_{nm}\delta_{ml}\right\}\sin[k_l L_x], \tag{28}$$

whereas for the external ($x > L_x$) region

$$\begin{aligned}\psi_k(\mathbf{r}) = {} & C_l \sin\left[\frac{l\pi y}{L_y}\right]\sin[k_l x] - \gamma C_l \\ & \times \left\{\sum_{n,m=1}^{\infty} \sin\left[\frac{n\pi y}{L_y}\right]\exp[\pm \mathrm{i}k_n x]\frac{(k_m/k_n)\sin[k_n L_x]L_y^2}{k_m L_y + \gamma\ \sin[k_m L_x]\exp[\pm \mathrm{i}k_m L_x]}\right. \\ & \left.\times \int_0^1\int_0^1 \mathrm{d}t_b\,\mathrm{d}t_a \varphi_n(L_y t_b)\varphi_m(L_y t_b)\varphi_m(L_y t_a)\varphi_l(L_y t_a)\right\}\sin[k_l L_x] \\ = {} & C_l \sin\left[\frac{l\pi y}{L_y}\right]\sin[k_l x] - \left\{\gamma C_l \sum_{n,m=1}^{\infty}\sin\left[\frac{n\pi y}{L_y}\right]\exp[\pm \mathrm{i}k_n x]\right. \\ & \left.\times \frac{(k_m/k_n)\sin[k_n L_x]}{k_m L_y + \gamma\ \sin[k_m L_x]\exp[\pm \mathrm{i}k_m L_x]}\delta_{nm}\delta_{ml}\right\}\sin[k_l L_x]. \end{aligned} \tag{29}$$

If $k$ is such that $k_l L_x = j\pi$ ($j = 1, 2, \ldots$) then $\sin[k_l L_x] = 0$ and either from equation (28) or from equation (29) we find that $\psi_k(\mathbf{r}) = \phi_k(\mathbf{r})$ regardless the permeability parameter $\gamma$. This again is due to the TP (see the discussion after equation (26)).

For $\sin[k_l L_x] \neq 0$, we have for $x < L_x$

$$\psi_k(\mathbf{r}) = A(k_l;\gamma)\phi_k(\mathbf{r}) = \mathcal{A}(k_l;\gamma)C_l \sin\left[\frac{l\pi y}{L_y}\right]\sin[k_l x] \tag{30}$$

and for $x > L_x$

$$\psi_k(\mathbf{r}) = A(k_l;\gamma)C_l \sin\left[\frac{l\pi y}{L_y}\right]\left\{\sin[k_l x] + \frac{\gamma\ \sin[k_l L_x]}{k_l L_x}\ \sin[k_l(x - L_x)]\right\}, \tag{31}$$

where

$$A(k_l;\gamma) = \frac{k_l L_x}{k_l L_x + \gamma\ \sin[k_l L_x]\exp[\pm \mathrm{i}k_l L_x]}. \tag{32}$$

As it should be $\psi_k(\mathbf{r})$ is continuous at $x = L_x$.

An interesting consequence of the above geometrical configuration is the emergence of quasi-bound states associated to the one-sided leaking ($\mathcal{C}$) rectangular structure placed at the closed end of the semi-infinite waveguide. Actually, there are different procedures [44, 45] to generate resonances in cavities and closed waveguides [18]. For instance, one goal is try to enhance the intensity of the resulting stationary electromagnetic modes [44]. Although far from being a practical realization, our present setup might constitute a workable idea towards such aim. Indeed, for $x < L_x$ (equation (30)) the presence of $\mathcal{C}$ leads to an amplitude factor $A(k_l;\gamma)$ (equation (32)) for the waveguide natural eigenstate $\phi_k$. By rewriting $\gamma$ in terms of the probability transmission $P_t$ and $k_l$ (see section 2), and for the incident wavelength $\lambda_l = 2\pi/k_l$, we plot in figure 3 $|A|^2$ as function of $\lambda_l/L_x$ for four values of $P_t$, assuming the first $l = 1$ mode in the $y$ direction. For each $P_t$, clearly there are values of $\lambda_l/L_x$ for which $|A|^2$ is much higher than the reference unit amplitude, characterizing a great gain inside the waveguide. This phenomenon is considerably more pronounced for lower transmissivity through $\mathcal{C}$. But then, as expected the quasi-state resonances widths become much narrower.

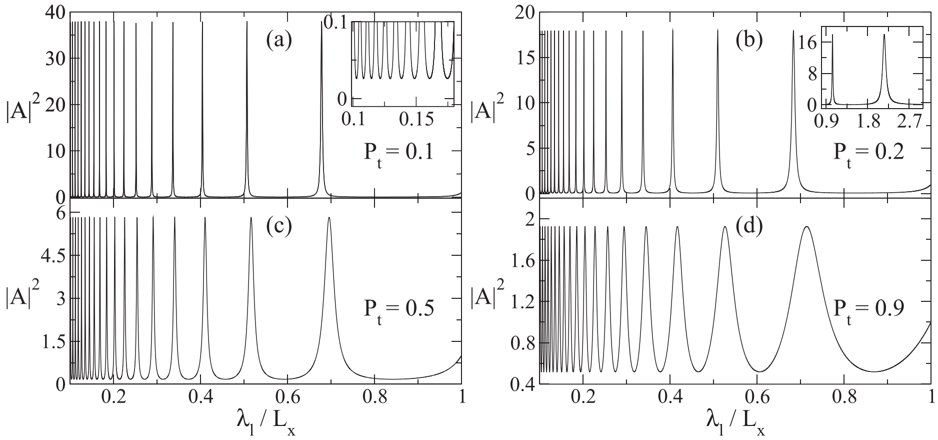


**Figure 3.** The modulus square of $A$, equation (32), as function of $\lambda_l/L_x$ (with $\lambda_l$ the incident wavelength along $x$) for four distinct values of the probability transmission $P_t$ across $\mathcal{C}$. Here $l = 1$ and $L_x = 1$. The peaks represent quasi-bound states resonances associated to the rectangular one side leaking structure, when the wave amplitude greatly increases. The inset in (a) illustrates that for $P_t > 0$, $|A|^2$ does not completely vanish for any value of $\lambda_l/L_x$ if $P_t > 0$. The inset in (b) exemplifies a general trend, the resonances tend to disappear for $\lambda_l/L_x$ of the order of few units. In (b) no important peaks are observed for $\lambda_l/L_x > 2.7$.

### 4.2. Numerical examples for distinct $\mathcal{C}$'s

Lastly we present few representative numerical examples. The aim is not to address extremely accurate simulational results or very detailed analysis for the shapes discussed. Instead, we shall illustrate the suitability and usefulness of the proposed BWM construction. A comprehensive study of potential applications for the BWM exploring the geometry of semi-infinite waveguides should be the subjected of a forthcoming, computationally-oriented, work.

We assume certain values for $\theta$ and $L_x$ such that $\mathcal{C}$ together with appropriate parts of the rectangular waveguide borders form distinct structures, see figure 2(b). We recall that the division of $\mathcal{C}$ into $N$ 'pieces' and the numerical calculation of $T$ and $T_\gamma$—which upon such discretization become $N \times N$ matrices [18]—follow the exact same scheme outlined in [15]. The only difference is to substitute the 2D free space Green's function in section 2 by $G^{(+)}_{\text{rwg}}$,[5] with $\sum_n(\cdot)$ in equation (14) truncated at $n = N^*$ (see below). The states $\psi_k$, equation (2), are then obtained by usual numerical integration.

As in any boundary-like method [8, 9], for adequate convergence the previously mentioned $N$ partitioning of $\mathcal{C}$ must take into account the range of $\lambda = 2\pi/k$. We use the parameterization $N = \zeta P_{\mathcal{C}}/\lambda$, where $P_{\mathcal{C}}$ is the curve $\mathcal{C}$ perimeter. From some direct tests we have determined that $\zeta = 30$–$40$ ($\zeta = 14$–$20$) represents a proper compromise between inexpensive simulations and fair numerical precision when $k < 20$ ($k \sim 100$). Note that by fair here one should have clear the type of application, therefore the necessary accuracy for the sought results.

In particular, concerning eigenvalues of closed $\mathcal{C}$'s with Dirichlet BCs (billiards), to compare the present BWM formulation with others methods, say, in terms of $\zeta$, one must bear in mind that the present discretization takes place only for a part of the structure frontiers,

[5] To determine the inside billiards eigenstates one can use either the $(+)$ or the $(-)$ Green's function. But to treat $\mathcal{C}$ as a scatter for the outside waveguide states, the outgoing $(+)$ is a better choice.

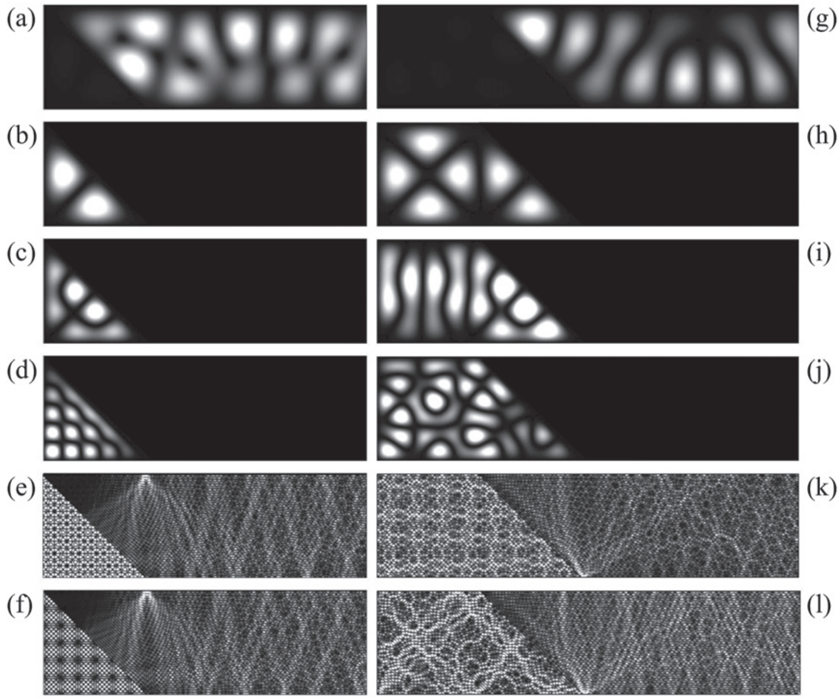


**Figure 4.** Density plots of the numerically calculated $|\psi_k(\mathbf{r})|^2$ for $\theta = 3\pi/4$ and $L_x = L_y$ (first) and $L_x = 2L_y$ (second) columns, with $L_y = \sqrt{2}$. Such parameters result, respectively, in 45°–45° right triangle and square −45°trapezium shapes (cf, figure 2). The $k$'s in (a) and (g) do not correspond to eigenwavenumbers, so the BWM leads to null solutions within the billiard region. The plots (b)–(d) and (h)–(j) display only the inside eigenfunctions—the outside waveguide states are deliberated omitted for a better visualization. In (e), (f), (k) and (l), both the billiard eigenstates and the outside scattered $\phi_k$'s are shown (for these four examples $N_k = 45$ in equation (33), but the $\phi_k$'s are not the same because the small difference between the $k$'s). The specific $k$'s are: (a) 6.5000, (b) 7.0279, (c) 11.3321, (d) 17.3577, (e) 100.6681, (f) 100.8641, (g) 6.5000, (h) 7.0259, (i) 10.2191, (j) 14.4870, (k) 100.3652, (l) 100.0923. The $|\psi_k(\mathbf{r})|^2$ for the right triangles in practice perfectly reproduce the corresponding exact solutions in equation (34), with the quantum numbers given in table 1.

whereas in different approaches, the discretization is done along the entire billiard borders. Then, a practical way to contrast protocols—of course, for same typical spatial sizes (e.g., billiard area) and $k$ ranges—is to verify the numerical precision given the $N$'s used. For example, for the very effective extended boundary integral method proposed in [46], for $k \sim 70$ the authors use $\zeta = 12$, a similar discretization procedure to ours, but for a Monza billiard of area around 7. The goal there is to resolve doublets, quasi-degenerate states, and thus the numerical precision needed (and indeed obtained) is much higher than ours for equal $N$'s. It is also worth mentioning the very powerful approach developed in [47]. By means of scaling considerations, one can obtain highly excited states of billiards in a narrow energy range with impressive very small error. In fact, such technique has been considered to calculate the spectrum of chaotic triangular billiards [48] with the number of levels in the order of $10^6$.

The BWM for waveguides, when employed to compute billiards eigenstates, does not display such a great numerical efficiency. Nonetheless, ours should not be viewed as a competing

**Table 1.** For all the right triangle billiard eigenstates in figure 4, the numerical $k$ and the exact $k_{pq}$, whose percentage difference is given by $\Delta k\%$. The sizes of the discretized $T$ matrices for the present ($N$) and for the free space ($N_{\mathrm{free}}$) BWM formulations are also given. For each example, the listed $N$ and $N_{\mathrm{free}}$ lead to the same numerical precision. The percentage difference $\Delta k_{\mathrm{sup}}\%$ ($\Delta k_{\mathrm{inf}}\%$) between $k_{pq}$ and the exact eigenwavenumber mode just above (below) $k_{pq}$ is also shown. Contrasting $\Delta k\%$ with $\Delta k_{\mathrm{inf/sup}}\%$, it becomes clear that the method properly resolves the individual levels.

| Figure 4 | $k_{pq}(p,q)$ | $(\Delta k_{\mathrm{inf}}\%)$ and $(\Delta k_{\mathrm{sup}}\%)$ | $k$ $(\Delta k\%)$ | $N$ | $N_{\mathrm{free}}$ |
|---|---|---|---|---|---|
| (b) | 07.0248 (1, 3) | (41.42%) and (12.29%) | 07.0279 (0.04%) | 224 | 601 |
| (c) | 11.3272 (1, 5) | (1.98%) and (5.31%) | 11.3321 (0.04%) | 219 | 669 |
| (d) | 17.3500 (5, 6) | (2.55%) and (3.12%) | 17.3577 (0.04%) | 218 | 666 |
| (e) | 100.6536 (17, 42) | (0.07%) and (0.07%) | 100.6681 (0.01%) | 680 | 1933 |
| (f) | 100.8495 (6, 45) | (0.10%) and (0.12%) | 100.8641 (0.01%) | 680 | 1939 |

protocol to those in [46, 47]. Indeed, as expected different methods tend to be more fitted to distinct purposes. The mentioned procedures are ideal to determine large number of levels with high accuracy. On the other hand, both the traditional and the present BWM may be more appropriate, e.g., to investigate the spectrum features of families of shapes [49], billiards with leaking borders and small structures coupled to waveguides [18].

Regarding the truncation of $G^{(+)}_{\mathrm{rwg}}$, as a rule of thumb we have found that for a given $k$ we can set $N^* = N_k + 2N$, with $N_k$ the largest integer for which $k^2 - N_k^2\pi^2/L_y^2$ is real. Hence, in the numerics we should consider $2N$ evanescent modes [41] for the rectangular semi-infinite waveguide Green's function. We further observe that the sum in equation (14) runs over simple trigonometric and exponential functions, so very easy to deal with computationally. Moreover, owned to the particular dependence of the Green's function on $k$—associated only to the $x$ coordinate in the term $\sin[k_n x_<]\exp[\pm \mathrm{i} k_n x_>]$, see equation (14)—the fact that $G^{(+)}_{\mathrm{rect}}$ is written as a series expansion could be strongly mitigated through well-established meshing and vectorization techniques [50]. However, for the examples next such type of algorithm optimization is not indeed required.

To facilitate finding the billiard systems eigenstates, it is appropriate to choose a 'seed' state $\phi_k$ [12] with a large number of modes in the $y$ direction [25]. Thus, we assume the following steady state for the waveguide in the absence of $\mathcal{C}$

$$\phi_k(\mathbf{r}) = C \sum_{l=1}^{N_k} \sin[l\pi y/L_y] \sin\left[\sqrt{(k^2 - l^2\pi^2/L_y^2)}x\right]. \tag{33}$$

For convenience, we set the normalization constant $C$ to 1. In all which follows we specify the geometric parameters and $k$ values and then display density plots of the corresponding $|\psi_k|^2$, with $\psi_k$ given by equation (2). Brighter (darker) regions indicate a higher (smaller) wavefunction amplitude. The simulations have been performed with a homemade Fortran code and the pictures drawn using the software Mathematica.

In figure 4 we have $\theta = 3\pi/4$ and $L_x = L_y$ in the first column and $L_x = 2L_y$ in the second column with, both with $L_y = \sqrt{2}$. Thus, the corresponding billiards are the classically integrable 45°–45° right triangle of area 1, whose quantum solutions read [51] (for $p \neq q$ positive integers)

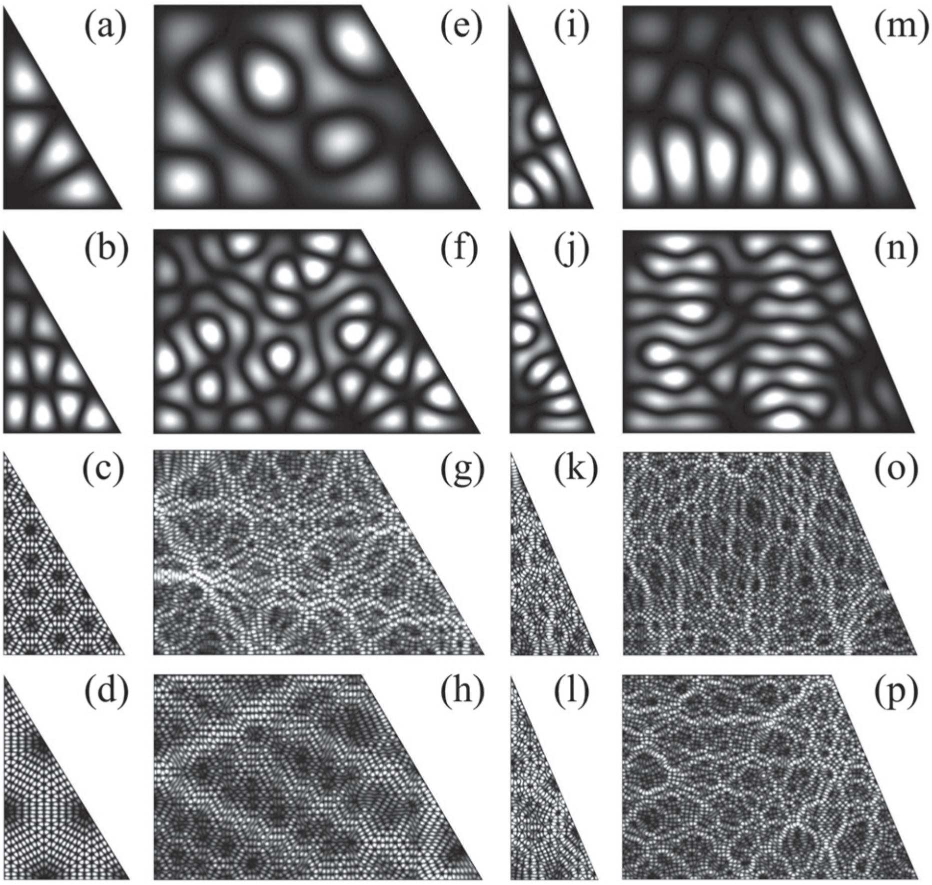


**Figure 5.** Density plots of the absolute square of some numerical eigenstates. From (a) to (h) $\theta = 2\pi/3$, $L_y = 12^{1/4}$ and $L_x = (4/3)^{1/4}$ for the 60°–30° right triangle and $L_x = 12^{1/4} + (4/3)^{1/4}$ for the square −60° trapezium. From (i) to (p) $\theta = 5\pi/8$, $L_y = \sqrt{2\tan[3\pi/8]}$ and $L_x = \sqrt{2/\tan[3\pi/8]}$ for the 67.5°–22.5° right triangle and $L_x = \sqrt{2\tan[3\pi/8]} + \sqrt{2/\tan[3\pi/8]}$ for the square −67.5° trapezium. The specific $k$'s are: (a) 10.3182, (b) 15.2297, (c) 100.4155, (d) 100.5292, (e) 8.1563, (f) 15.2142, (g) 100.4206, (h) 100.6029 (i) 13.3615, (j) 15.9067, (k) 100.7009, (l) 100.8680, (m) 8.2714, (n) 13.1436, (o) 100.2544, (p) 100.0844.

$$\psi_{pq}(x,y) = \frac{1}{L_y}\left(\sin\left[\frac{p\pi x}{L_y}\right]\sin\left[\frac{q\pi(L_y-y)}{L_y}\right] - \sin\left[\frac{q\pi x}{L_y}\right]\sin\left[\frac{p\pi(L_y-y)}{L_y}\right]\right) \tag{34}$$

and the classically quasi-integrable square −45° trapezium [52–54] of genus 2 [55] and area 3, for which a fraction of the quantum eigenstates (those with a node along $x = L_y$) are also given by equation (34), but with the substitution $x \to x + L_y$ and a distinct normalization constant. Of course, outside the billiard we have a rectangular semi-infinite waveguide with a diagonal-wall ending.

In table 1 we compare the numerical and analytical eigenwavenumbers for the right triangle billiards of figure 4, plots (b)–(f). Using the above heuristics to set the size of the discretized $T$ matrices, we also show the corresponding $N$ values. Note that the $\Delta k\%$'s between the exact

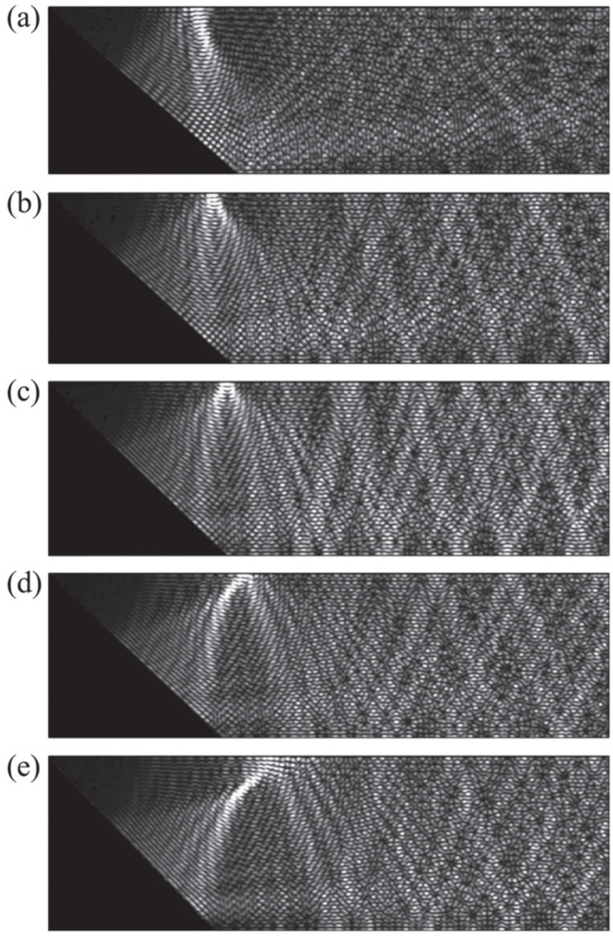


**Figure 6.** Density plots of the scattering solutions $|\psi_k(\mathbf{r})|^2$ in the waveguide region for $k = 100.6320$ and a right triangle with $\theta = \pi/2 + \phi$, $L_y = \sqrt{2\tan[\phi]}$, $L_x = \sqrt{2/\tan[\phi]}$ and (a) $\phi = 40^\circ$, (b) $\phi = 43^\circ$, (c) $\phi = 45^\circ$, (d) $\phi = 47^\circ$, (e) $\phi = 50^\circ$.

and numerical $k$'s are very reasonable given the relatively small $N$'s and the elementary truncation procedure for the Green's function. Moreover, the numerical error $\Delta k\%$ is considerably smaller than the separation between two successive neighbor levels (observe the third and fourth columns in table 1). We also contrast the present $N$'s with those from the usual BWM (i.e., using a 2D free space Green's function and then $\mathcal{C}$ being the full billiard contour) yielding a same numerical accuracy. At least concerning the necessary size of the $T$ matrix, the waveguide prescription is clearly an advantage. Finally, it may be the case that to resolve neighbor levels in a certain $k$ interval (say $k \sim 100$), we need to consider larger $N$'s than those used for other levels in this same interval. For instance, suppose the four successive exact eigenwavenumbers $k_{17,42} = 100.6536$ ((e) in table 1) $< k_{30,34} = 100.7271 < k_{11,44} = 100.7516 < k_{6,45} = 100.8495$ ((f) in table 1). Note that $\Delta = k_{11,44} - k_{30,34} = 0.0245 \approx \overline{\delta}/2.5$ for the mean level spacing [56] $\overline{\delta} \approx 2\pi/(kA) = 0.0622$ (with $A = 1$ the billiard area and $k$ set to 101). Hence, in this specific situation we need to increase $N$ (from 680 in table 1) to numerically determine the close $k_{30,34}$ and $k_{11,44}$. Actually, for $N = 1300$ we find from the method $k_a = 100.7346$ for

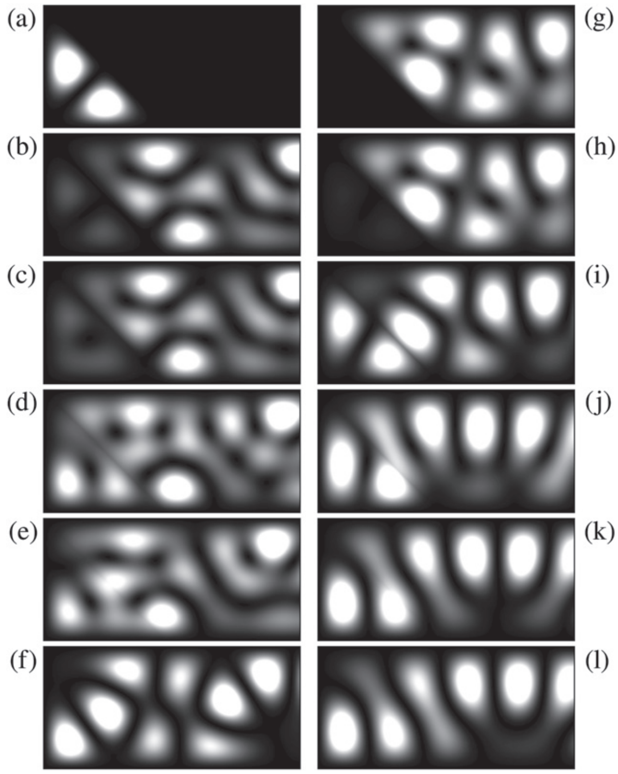


**Figure 7.** Density plots of $|\psi_k(\mathbf{r})|^2$ for the same 45°–45° right triangle configuration of figure 4, but for distinct permeabilities of $\mathcal{C}$. The wavenumber value in the left (right) column is $k = 7.0279$ ($k = 6.5000$), corresponding to the resonance (off-resonance) example in figure 4(b) (figure 4(a)). The probabilities of transmission $P_t$ through $\mathcal{C}$ (see section 2) are: (a) and (g) 0 (same than in figure 4), (b) and (h) 0.01 (c) and (i) 0.1, (d) and (j) 0.5, (e) and (k) 0.9, (f) and (l) 0.999.

$k_{30,34}$ (so that $k_{11,44} - k \approx 0.017$ and $k - k_{30,34} \approx 0.007$) and $k_b = 100.7592$ for $k_{11,44}$ (so that $k_{6,45} - k_b \approx 0.090$ and $k_b - k_{11,44} \approx 0.008$), thus sorting out these two levels.

Some trapezium eigenstates are depicted in figures 4(h)–(l). Since (h) displays a node along $x = L_y$, as already mentioned it corresponds to a solution in the form of equation (34) with $x \to x + L_y$ (hence extending to the whole trapezium billiard interior region). Indeed, it is not difficult to realize that $\psi_n$ in (h) is directly obtained from the triangle eigenstate in (b) by a back folding through $x = L_y$ and then a diagonal folding through $x = y$. Of course, they should have exactly the same energy. The observed small difference between the $k$'s (see the figure 4 caption) is due to the numerical approximation. By using in both cases $N = 600$, one gets the much closer values (b) $k = 7.0259$ and (h) $k = 7.0253$. We also show in figures 4(e), (f), (k) and (l) how $\phi_k$, equation (33), is scattered off by the wall $\mathcal{C}$ within the waveguide (refer to equation (6)). Observe that the interference pattern difference of (e) and (f) to (k) and (l) is related to the two distinct positions of $\mathcal{C}$ along the $x$ axis (an effect we have checked by shifting around $\mathcal{C}$, but do not show here). The subtler but still noticeable distinction between (e) and (f) and between (k) and (l) is due to the specific $k$ values.

In figure 5 we display some extra numerically calculated eigenstates for right triangles (of area 1) and square trapezium (of area 3) billiards. In the first, second, third and fourth columns we have, respectively, a $60°–30°$ right triangle, a square $-60°$ trapezium, a $67.5°–22.5°$ right triangle and a square $-67.5°$ trapezium. For the specific geometric sizes see the caption of figure 5. Only the $60°–30°$ right triangle is classically integrable, the other three are quasi-integrable (of genus 2, 2 and 4). This fact becomes qualitatively explicit in the plots. Indeed, for the $60°–30°$ right triangle billiard observe the very regular and symmetric morphologies of the eigenstates—given as linear combination of a small number of simple sine functions, see, e.g., reference [51]—therefore contrasting with the other examples, specially for higher $k$ values.

We have seen in figure 4 that the scattering patterns along the waveguide depends on the exact location of $\mathcal{C}$. Of course, they also must depend on the inclination $\theta$ of $\mathcal{C}$. In figure 6 we show the scattering solutions outside the right triangle billiard structure (for which we maintain a fixed area of 1), considering five values for $\theta = \pi/2 + \phi$. In all cases $k = 100.6320$. We clearly observe a qualitative change for $|\psi_k(\mathbf{r})|^2$ as $\phi$ ranges from $40°$ to $50°$. Interestingly, there is a very intense constructive interference spot in the superior waveguide wall, which tends to move to the right as $\theta$ increases. So, $\mathcal{C}$ is acting as a kind of focalizing mirror for the incident $\phi_k$.

Finally, we give a numerical example of $\mathcal{C}$ a permeable wall barrier, characterized by a transmission probability $P_t$, section 2. We consider the geometry and $k$ values of figures 4(a) and (b), with this latter $k$ representing then a right triangle eigenwavenumber. The results for $P_t$ equals to 0, 0.01, 0.1, 0.5, 0.9 and 0.999 are shown, respectively, from rows 1 to 6 in figure 7. Obviously, for $P_t = 0$, the $|\psi_k|^2$'s are the same than those in figures 4(a) and (b). As $P_t$ increases, resulting in a consequent greater leakage through $\mathcal{C}$, the intensity of the wavefunction inside the right triangular structure becomes higher. For $P_t = 0.999$, practically the wall becomes transparent and we have a continuous steady state solution along the whole rectangular waveguide region.

## 5. Conclusion

The BWM is a generic protocol to solve boundary value problems for wave equations. But like the majority of the approaches to deal with such classes of systems, some technical difficulties may arise depending on the borders $\mathcal{C}$ characteristics. An advantage of the BWM is that in many instances one has a considerable freedom for choosing the method 'free' Green's function $G_0$. We have then explored this key feature of the BWM and developed a formulation based on the $G_0$ for a semi-infinite waveguide.

We have considered the explicit case of a rectangular semi-infinite waveguide, which finds interesting usages as discussed along the work. Indeed, we have illustrated certain trademarks of our construction presenting distinct analytic and numeric examples, assuming structures like rectangular, triangular and trapezoidal billiards, with Dirichlet and leaking BCs. We also have discussed the scattering solutions in the interior of our rectangular semi-infinite waveguide. Numerically, we have presented a very simple procedure to calculate $G_0$ and the $T$ matrix, enough for simple utilizations. However, more elaborated algorithms would certainly improve its computational effectiveness. In particular, to obtain the eigenvalues of closed billiards for high $k$'s (for the shapes and typical spatial sizes addressed, meaning $k$ greater than 100) the procedure may become, numerically, less efficient. This is not a typical property of the BWM [12, 15]. Most likely, such behavior might be associated to the necessity of including evanescent modes in the $G_0$ calculation, well known to be a trick factor to solve billiard problems [57, 58]—nonetheless inevitable for the waveguide here (see, e.g., reference [58]).

We finally should emphasize that one is not restricted to a particular waveguide geometry. Distinct waveguides potentially could increase the possibility of both analytical and numerical results for many other $\mathcal{C}$'s and even improve the numerical accuracy for billiards (say, by demanding smaller $N$'s). We hope our analysis can motivate further studies using the BWM in connection with waveguides.

## Acknowledgments

We would like to thank a research Grant from CNPq 304532/2019-3 (da Luz) and scholarships from Capes (Azevedo and Teston) and CNPq (Sales).

## Data availability statement

All data that support the findings of this study are included within the article (and any supplementary files).

## Appendix A. The rectangular box Green function

For completeness we show how to obtain the Green function $G_{\text{box}}$ for a 2D box [40] from $G^{(\pm)}_{\text{rwg}}$. Recall that for $G_{\text{box}}$, we must assume $0 < x < L_x$ and $0 < y < L_y$, with Dirichlet BCs at $x = 0, L_x$ and $y = 0, L_y$ and that $G^{(\pm)}_{\text{rwg}}$ already satisfy these conditions at $x = 0$ and $y = 0, L_y$.

For $x > x_0$, $G^{(\pm)}_{\text{rwg}}$ represents a particle propagating to the right $(+)$ (left $(-)$) along $x$. Since we are looking for a 'stationary' Green function, it is very reasonable to write $G_{\text{box}}$ as a linear combination of these two $G$'s, but with necessary changes in the phases of each mode $n$ composing $G^{(\pm)}_{\text{rwg}}$. To achieve this, we implement the rescaling $F^{(\pm)}_n \to c^{(\pm)}_n(k_n; L_x)F^{(\pm)}_n$—therefore not altering the action of the derivatives on $F_n$—in the expressions for $G^{(\pm)}_{\text{rwg}}$ (hereafter labeled $G^{(\pm)}_{\text{rwg,c}}$) and consider $G^{(+)}_{\text{rwg,c}} - G^{(-)}_{\text{rwg,c}}$. If for $c^{(\pm)}_n$ we take $(\mathrm{i}/2)\exp[\mp \mathrm{i}k_nL_x]$, it is direct to show that the $x_>$ dependence of $G^{(+)}_{\text{rwg,c}} - G^{(-)}_{\text{rwg,c}}$ becomes $\sin[k_n(L_x - x_>)]$, hence $G^{(+)}_{\text{rwg,c}} - G^{(-)}_{\text{rwg,c}}$ is null either for $x = L_x$ or for $x_0 = L_x$.

Nevertheless, from the previous procedures, we find that in this case $(\nabla^2 + k^2)(G^{(+)}_{\text{rwg,c}} - G^{(-)}_{\text{rwg,c}}) = \sin[k_nL_x]\delta(x - x_0)\delta(y - y_0)$. Finally, to eliminate such sine prefactor for the $\delta$'s, we just redefine $c^{(\pm)}_n = (\mathrm{i}/2)\exp[\mp \mathrm{i}k_nL_x]/\sin[k_nL_x]$. Then, $G_{\text{box}} = G^{(+)}_{\text{rect,c}} - G^{(-)}_{\text{rect,c}}$ yields

$$G_{\text{box}} = \sum_{n=1}^{\infty} \varphi^{(L_y)}_n(y)\varphi^{(L_y)}_n(y_0)\frac{(-1)}{k_n\,\sin[k_nL_x]}\,\sin[k_nx_<]\sin[k_n(L_x - x_>)]. \tag{A.1}$$

It remains to prove that the above expression is actually the well known correct Green function for a particle in a 2D box [39, 40]. For so, we follow a method developed in [59]. Since $\sin[u]\sin[v] = (\cos[u - v] - \cos[u + v])/2$ and from 1.445–6 in [60], namely, $\sum_{m=1}^{\infty}\cos[mz]/(m^2 - \alpha^2) = 1/(2\alpha^2) - \pi\,\cos[\alpha(\pi - z)]/(2\alpha\,\sin[\alpha\pi])$, we can write (by identifying $\alpha = k_nL_x/\pi$)

$$
\begin{aligned}
-\frac{\sin[k_n x_<]\sin[k_n(L_x - x_>)]}{k_n\ \sin[k_n L_x]} &= \frac{1}{2k_n\ \sin[k_n L_x]}\big(\cos[k_n(L_x - |x - x_0|)] \\
&\quad - \cos[k_n(L_x - (x + x_0))]\big) \\
&= \frac{1}{L_x}\sum_{m=1}^{\infty}(k_n^2 - m^2\pi^2/L_x^2)^{-1} \\
&\quad \times \big(\cos[m\pi(x - x_0)/L_x] - \cos[m\pi(x + x_0)/L_x]\big) \\
&= \frac{2}{L_x}\sum_{m=1}^{\infty}\frac{\sin[m\pi x/L_x]\sin[m\pi x_0/L_x]}{(k^2 - n^2\pi^2/L_y^2 - m^2\pi^2/L_x^2)},
\end{aligned} \tag{A.2}
$$

such that

$$
G_{\text{box}} = \sum_{n,m=1}^{\infty}\frac{\varphi_n^{(L_y)}(y)\varphi_n^{(L_y)}(y_0)\varphi_m^{(L_x)}(x)\varphi_m^{(L_x)}(x_0)}{k^2 - n^2\pi^2/L_y^2 - m^2\pi^2/L_x^2}, \tag{A.3}
$$

which is the exact Green function for the mentioned problem as found, e.g., in [39, 40].

## ORCID iDs

A L Azevedo https://orcid.org/0000-0001-9405-658X
M R Sales https://orcid.org/0000-0002-1121-6371
M G E da Luz https://orcid.org/0000-0003-3865-2621

## References

[1] Stakgold I 2000 *Boundary Value Problems of Mathematical Physics* (*Classics in Applied Mathematics* vol 29) (Philadelphia, PA: SIAM)
[2] Willatzen M and Voon L C L Y 2011 *Separable Boundary-Value Problems in Physics* (New York: Wiley)
[3] Keller H B 1992 *Numerical Methods for Two-Point Boundary-Value Problems* (New York: Dover)
[4] Goldberg M A (ed) 1998 *Boundary Integral Methods: Numerical and Mathematical Aspects* (Southampton: WIT Press)
[5] Powers D L 2009 *Boundary Value Problems* 6th edn (New York: Academic)
[6] Stakgold I and Holst M 2011 *Green's Functions and Boundary Value Problems* 3rd edn (New York: Wiley)
[7] Chowdhury S, Das P K and Faruque S B 2018 *Numerical Solutions of Boundary Value Problems with Finite Difference Method* (Bristol: IOP Publishing)
[8] Yakimov A S 2016 *Analytical Solution Methods for Boundary Value Problems* (New York: Academic)
[9] Boutayeb A and Chetouani A 2006 A mini-review of numerical methods for high-order problems *Int. J. Comput. Math.* **84** 563–79
[10] Newton R G 2013 *Scattering Theory of Waves and Particles* 2nd edn (New York: Dover)
[11] Bleistein N 1984 *Mathematical Methods for Wave Phenomena* (New York: Academic)
[12] da Luz M G E, Lupu-Sax A S and Heller E J 1997 Quantum scattering from arbitrary boundaries *Phys. Rev.* E **56** 2496–507
[13] Nagler J, Krieger M, Linke M, Schonke J and Wiersig J 2007 Leaking billiards *Phys. Rev.* E **75** 046204
[14] Joachain C J 1984 *Quantum Collision Theory* (Amsterdam: North-Holland)
[15] Zanetti F M, Vicentini E and da Luz M G E 2008 Eigenstates and scattering solutions for billiard problems: a boundary wall approach *Ann. Phys., NY* **323** 1644–76

[16] Maioli A C and Schmidt A G M 2018 Exact solution to Lippmann–Schwinger equation for a circular billiard *J. Math. Phys.* **59** 122102

[17] Maioli A C and Schmidt A G M 2019 Exact solution to the Lippmann–Schwinger equation for an elliptical billiard *Physica* E **111** 51–62

[18] Zanetti F M and da Luz M G E 2012 Determining and characterizing families of electronic resonance states in open and closed coupled cavities *Eur. Phys. J.* B **85** 202

[19] Schmidt A G M, Maioli A C and Azado P C 2020 Exact solution to the Lippmann–Schwinger equation for a spheroidal barrier *J. Quant. Spectrosc. Radiat. Transfer* **253** 107154

[20] Katine J A, Eriksson M A, Adourian A S, Westervelt R M, Edwards J D, Lupu-Sax A, Heller E J, Campman K L and Gossard A C 1997 Point contact conductance of an open resonator *Phys. Rev. Lett.* **79** 4806–9

[21] Vaishnav J Y, Itsara A and Heller E J 2006 Hall of mirrors scattering from an impurity in a quantum wire *Phys. Rev.* B **73** 115331

[22] Vaishnav J Y, Wall J D and Heller E J 2007 Matter waves scattering and guiding by atomic arrays *Phys. Rev.* A **76** 013620

[23] Parimi P V, Lu W T, Vodo P, Sokoloff J, Derov J S and Sridhar S 2004 Negative refraction and left-handed electromagnetism in microwave photonic crystals *Phys. Rev. Lett.* **92** 127401

[24] Macedo A G, Zanetti F, Mikowski A, Hummelen J C, Lepienski C M, da Luz M G E and Roman L S 2008 Improving light harvesting in polymer photodetector devices through nanoindented metal mask films *J. Appl. Phys.* **104** 033714

[25] Zanetti F M, Lyra M L, de Moura F A B F and da Luz M G E 2009 Resonant scattering states in 2D nanostructured waveguides: a boundary wall approach *J. Phys. B: At. Mol. Opt. Phys.* **42** 025402

[26] Garcia-Garcia H and Gutiérrez-Vega J C 2014 Scalar wave scattering in spherical cavity resonator with conical channels *J. Opt. Soc. Am.* A **31** 246–52

[27] Garcia-Garcia H and Gutiérrez-Vega J C 2012 Tunneling phenomena in the open elliptic quantum billiard *Phys. Rev.* E **86** 016210

[28] Nunes A, Zanetti F M and Lyra M L 2016 Switching of transmission resonances in a two-channels coupler: a boundary wall method scattering study *Ann. Phys., NY* **373** 707–16

[29] Levitan B M 1987 *Inverse Sturm–Liouville Problems* (Utrecht: VNU Science Press)

[30] Cabada A 2014 *Green's Functions in the Theory of Ordinary Differential Equations* (New York: Springer)

[31] Duffy D G 2015 *Green's Functions with Applications* 2nd edn (Boca Raton, FL: CRC Press)

[32] Sbailò L and Noé F 2017 An efficient multi-scale Green's function reaction dynamics scheme *J. Chem. Phys.* **147** 184106

[33] Zanetti F M, Kuhn J, Delben G J, Cheng B K and da Luz M G E 2006 Classifying the general family of 1D point interactions: a scattering approach *J. Phys. A: Math. Gen.* **39** 2493–508

[34] Dietz B and Smilansky U 1993 A scattering approach to the quantization of billiards- the inside-outside duality *Chaos* **3** 581–9

[35] Primack H, Schanz H, Smilansky U and Ussishkin I 1997 Penumbra diffraction in the semiclassical quantization of concave billiards *J. Phys. A: Math. Gen.* **30** 6693–723

[36] Stöckmann H-J 2008 Scattering properties of chaotic microwave resonators *AIP Conf. Proc.* **1076** 223

[37] Wirzba A 1992 Validity of the semiclassical periodic orbit approximation in the two- and three-disk problems *Chaos* **2** 77–83

[38] Lu W, Viola L, Pance K, Rose M and Sridhar S 2000 Microwave study of quantumn-disk scattering *Phys. Rev.* E **61** 3652–63

[39] Barton G 1999 *Elements of Green's Functions and Propagation* (Oxford: Oxford University Press)

[40] Wyld H W 1999 *Mathematical Methods for Physicists* 2nd edn (Boca Raton, FL: CRC Press)

[41] Berry M V 1994 Evanescent and real waves in quantum billiards and Gaussian beams *J. Phys. A: Math. Gen.* **27** L391–8

[42] Eckmann J-P and Pillet C-A 1995 Spectral duality for planar billiards *Commun. Math. Phys.* **170** 283–313

[43] Dietz B, Eckmann J-P, Pillet C-A, Smilansky U and Ussishkin I 1995 Inside-outside duality for planar billiards: a numerical study *Phys. Rev.* E **51** 4222–31

[44] Ehrhardt M (ed) 2010 *Wave Propagation in Periodic Media: Analysis, Numerical Techniques and Practical Applications* vol 1 (Sharjah: Bentham Science Publishers)

[45] Nasr M H, Othman M A K, Eshrah I A and Abuelfadl T M 2017 Solution of cavity resonance and waveguide scattering problems using the eigenmode projection technique *J. Appl. Phys.* **121** 143105
[46] Veble G, Prosen T and Robnik M 2007 Expanded boundary integral method and chaotic time-reversal doublets in quantum billiards *New J. Phys.* **9** 15
[47] Vergini E and Saraceno M 1995 Calculation by scaling of highly excited states of billiards *Phys. Rev.* E **52** 2204–7
[48] Lozej Č, Casati G and Prosen T 2022 Quantum chaos in triangular billiards *Phys. Rev. Res.* **4** 013138
[49] Sales M R, Azevedo A L, Teston F, da Luz M G E and Zanetti F M 2021 Soliton-like structures in the spectrum and the corresponding eigenstates morphology for the quantum desymmetrized Sinai billiard *Chaos* **31** 113122
[50] Hansen G A, Douglass R W and Zardecki A 2005 *Mesh Enhancement* (Singapore: World Scientific)
[51] Schachner H C and Obermair G M 1994 Quantum billiards in the shape of right triangles *Z. Phys.* B **95** 113–9
[52] Richens P J and Berry M V 1981 Pseudointegrable systems in classical and quantum mechanics *Physica* D **2** 495–512
[53] Grebenkov D S and Nguyen B-T 2013 Geometrical structure of Laplacian eigenfunctions *SIAM Rev.* **55** 601–67
[54] Lu Z and Rowlett J 2015 The sound of symmetry *Am. Math. Mon.* **122** 815–35
[55] Zyczkowski K 1992 Classical and quantum billiards: integrable, nonintegrable and pseudo-integrable *Acta Phys. Pol.* B **23** 245–70
[56] Berry M V and Howls C J 1994 High orders of the Weyl expansion for quantum billiards: resurgence of periodic orbits, and the Stokes phenomenon *Proc. R. Soc.* A **447** 527–55
[57] Okada Y, Shudo A, Tasaki S and Harayama T 2005 On the boundary element method for billiards with corners *J. Phys. A: Math. Gen.* **38** 6675–88
[58] Espinoza O J S and de Almeida A M O 1997 Bogomolny section for the stadium: I. Quantum theory *J. Phys. A: Math. Gen.* **30** 7301–13
[59] Lupu-Sax A 1998 Quantum scattering theory and applications *Doctor Thesis* Harvard University, Cambridge, MA https://projects.iq.harvard.edu/files/hellergroup/files/adam_lupu_sax_thesis.pdf
[60] Gradshteyn I S and Ryzhik I M 2007 *Tables of Integrals, Series, and Products* ed A Jeffrey and D Zwillinger (New York: Academic)